ESTABLISHING AN AUTOMATED HEAT-SOURCE CALIBRATION FRAMEWORK

D. K. RISSAKI*, A. N.VASILEIOU*, M. C. SMITH*,
O. MURÁNSKY**, P. G. BENARDOS***,
G.-C. VOSNIAKOS***

**The University of Manchester, Department of Mechanical, Aerospace and Civil Engineering, Sackville Street, Manchester M139PL, UK*
***ANSTO, Institute of Materials Engineering, New Illawarra Road, Lucas Heights, NSW, Australia*
****National Technical University of Athens, School of Mechanical Engineering, Manufacturing Technology Laboratory, GR-15773 Athens, Greece*

DOI 10.3217/978-3-85125-968-1-12

ABSTRACT

Heat source model calibration is a critical step in the process of developing a weld model. This typically involves running a thermal analysis for various sets of welding input parameters (efficiency, heat source radii, etc), and comparing the simulation results against experimental data, including thermocouple traces and fusion zone boundaries. This trial-and-error approach takes time and requires user judgement. This work aims towards establishing an automation and optimisation framework for heat-source calibration. Exhaustive search, exploration of solution space, and identification of suitable metrics are implemented and applied for the automated heat source calibration of a previously validated arc welding benchmark.

Keywords: heat source calibration, automation, optimisation

INTRODUCTION

The heat source calibration procedure is a required step to perform finite element welding simulations. The aim of heat source calibration is the identification of realistic heat source parameters for a given welding procedure [1-3]. The heat source parameters include the heat efficiency, the type and size of heat source distribution and its vertical position. The heat source calibration is usually a computationally intensive procedure of trial-and-error, which requires user judgement because of the presence of multiple good solutions and lack of strict guidance for how to handle them. The automation and optimisation of heat source calibration would accelerate the process and would ensure that an optimal solution is found.

Numerous research papers have been focused on the automation and optimisation of heat source calibration, and applied optimisation algorithms to determine the appropriate combination of heat source distribution parameters and heat efficiency simultaneously [4-7] or just the heat source distribution parameters with fixed efficiency [8]. However, the heat efficiency can be determined prior to the heat source geometric parameters by using

experimental data from far-field thermocouples, that is thermocouples far from the weld centre line [9]. The separate determination of heat efficiency and heat source parameters would simplify the optimisation procedure, as the combinations of parameters that need to be examined to find the best solution vector would be significantly reduced. Moreover, the correct efficiency could be safely determined, rather than its correct value being lost in the potentially multiple good solutions of this multi-variable optimisation problem.

This paper aims to establish a framework for implementing this two-step optimisation process for heat source calibration, with the first step being the fixation of heat efficiency and the second the determination of heat source parameters. More specifically, using as case study the NeT project Task Group 4 (TG4) specimen [10-11], an exhaustive search was performed to evaluate the solution space and different metrics were assessed to identify the best strategy for implementing an automated optimised heat source calibration.

NET-TG4 SPECIMENS

The specimens that were used as a case study in this research are from NeT Task Group 4 (TG4) [10-11]. They are AISI 316L(N) austenitic stainless steel plates with a 3-pass TIG weld in a slot. The filler metal was of type AISI 316L, the travel speed was 76.2 mm/min and no weaving was used. With the same welding parameters, many identical mock-ups were fabricated by this Task Group. In the current research, the experimental thermocouple data used were from specimens named 2-1A and 3-1B, and the experimental fusion boundary was taken from the macrograph of the specimen named 1-2B (Fig. 1). Only the 1st pass was studied.

The experimental thermocouple data were obtained from 12 locations on each specimen, as shown in Fig. 2. The thermocouples at the start and stop ends were not included in the analysis of this research, to minimise the influence of starting and stopping effects and concentrate on quasi-steady-state conditions at the bead mid-length. Thus, only the mid-length thermocouples were used, that is TC2, TC5, TC10, TC11, TC12 on the front (welded) face and TC7, TC8, TC9 on the back face. The temperature increases (maximum temperature minus initial temperature) of these thermocouples were examined, to identify which ones can be considered far-field (adequately far from heat source to not be very influenced by the local heat source characteristics). The lowest temperature increases were experienced by TC5, TC7, TC8, TC12, as can be seen in Table 1. Thus, these thermocouples will be characterised as far-field. The rest of the thermocouples used in this study, that is TC2, TC9, TC10, TC11, experienced high temperature increases and will be characterised as near-field. The temperature increases were in accordance with the distance of thermocouples from the heat source. More specifically, the nearer the thermocouple position to the heat source the higher the temperature increase experienced. The nominal positions of thermocouples can be seen in Table 1. The actual positions measured after completion of welding were slightly different from nominal, and the estimated actual positions of thermocouples were used in the simulations of this study, as it can be seen in Table 1.

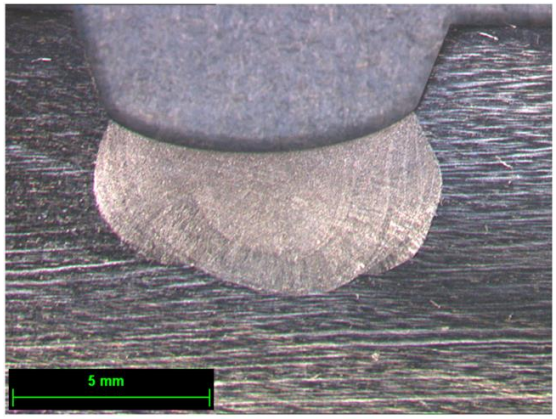

Fig. 1 Macrograph of 1-2B specimen that was used in this study as representative fusion boundary of NeT-TG4 benchmark [10]

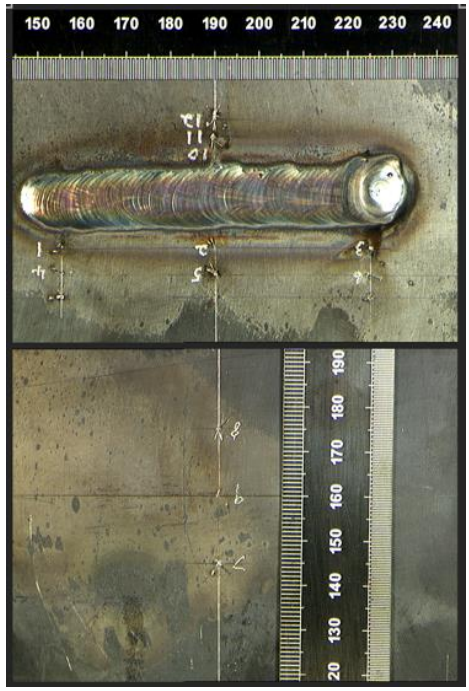

Fig. 2 Positioning of thermocouples on 3-1B mock-up [12]

Table 1 Experimental temperature increases ΔT (maximum - initial temperature) for thermocouples of specimens 2-1A and 3-1B and thermocouple nominal and estimated actual positions.

thermocouple	ΔT_{exp} 2-1A	ΔT_{exp} 3-1B	x nominal	y nominal	x actual 2-1A	x actual 3-1B	y actual 2-1A	y actual 3-1B
TC2	386.0	490.6	+13	0	12.4	12	0	0
TC5	246.3	265.7	+18	0	17.5	18.1	0	0
TC7	267.8	284.3	+15	18	14.3	15.1	18	18
TC8	284.9	255.7	-15	18	15.1	15.1	18	18
TC9	453.8	456.9	0	18	0.1	0.4	18	18
TC10	533.6	622.9	-9	0	8.9	8.6	0	0
TC11	350.5	371.6	-13	0	12.8	13.5	0	0
TC12	228.0	217.9	-18	0	18	17.1	0	0

EXHAUSTIVE SEARCH FOR HEAT EFFICIENCY

3-D steady-state analysis was performed with the FEAT-WMT heat source fitting tool [13]. The temperature dependent material properties and other weld modelling details can be found in [14-15], and were the same for all simulations of this study. The type of heat source used was ellipsoid, described by the Eq. (1):

$$q = \frac{Q}{Va} \exp -\{\left(\frac{x}{rl}\right)^2 + \left(\frac{y}{rv}\right)^2 + \left(\frac{z}{ra}\right)^2\} \quad (1)$$

where q is the power per unit volume, Q is the total power deposited, (x,y,z) is the geometric center of the distribution, and r_l, r_v, r_a are the radii of distribution in the lateral, vertical and axial directions respectively. The quantity Va is adjusted by the FEAT-WMT program automatically, so that the total power input is Q.

The three heat source distribution radii were first fixed to 1.0 mm size each, and many simulations run with different values of heat efficiency (from 10% to 100%). It was expected that the simulation temperature increase in far-field thermocouple points would not be much influenced by the arbitrary initial choice of heat source geometrical parameters. Therefore, it was expected that the heat efficiency could be quickly and accurately determined by comparing the temperature increases at these far-field points with the experimental ones, until an efficiency is found in which these two temperature increases are as close as possible. The metric used for comparison of the far-field temperature curves was the root mean square error (RMSE) of thermocouple increases, Eq. (2):

$$\text{RMSE} = \sqrt{\{\sum_{i=1}^{i=n} \frac{1}{n}\{(\Delta T_{TCi,sim} - \Delta T_{TCi,exp}) / \Delta T_{TCi,exp}\}^2\}} \quad (2)$$

where n is the number of far-field thermocouples (n = 4 for this study) and 'i' is the thermocouple numbering. ΔT denotes the temperature increase (maximum - initial temperature), and 'sim' refers to the simulation temperature increase, while 'exp' to the experimental one.

Both 2-1A and 3-1B specimens were found to have only one efficiency that minimises the RMSE. For the 2-1A specimen the efficiency that minimised the RMSE was 74% and for the 3-1B specimen it was 73%. Because of this slight disagreement, the average of the two RMSE was calculated and found that it was minimised at 74% efficiency, as it can be seen in Fig. 3. A similar triangular shape of graph was observed for the RMSE-efficiency graph of specimen 2-1A, of specimen 3-1B and in all other RMSE-efficiency graphs plotted in this study. Another method of using both specimens to determine the efficiency would be to use thermocouples from both specimens to calculate a single RMSE. One thing that should be considered in that case would be that the thermocouples used in each of the specimens should be equal in number, so that the specimen with more thermocouples does not dominate in the RMSE calculation. Both methods seem reasonable; however, they could lead to slightly different results.

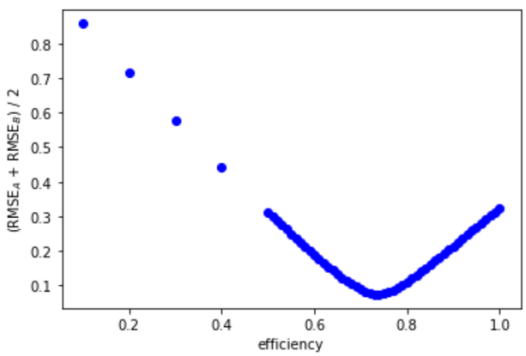

Fig. 3 Average RMSE of mock-ups 2-1A and 3-1B of far-field thermocouples for various values of heat efficiency

EXHAUSTIVE SEARCH FOR HEAT SOURCE RADII

After the initial fixation of efficiency to 74% based on experimental and simulation far-field thermocouple comparison, the solution space for best choice of heat source radii was examined. Based on previous experience within NeT-TG4, the interval of exploration that would possibly contain the optimal heat source radii solution was judged to be within the 1.0-3.0 mm interval for each of the three radii (r_a, r_l, r_v). Many simulations were run, with altogether having all possible combinations of heat source radii within the specified interval and with step of 0.1 mm. The efficiency was kept fixed for all these simulations at 74%.

A metric was developed to compare the experimental and simulation fusion boundary shapes automatically. Two mean square errors (MSE)[1] between the two fusion boundary shapes were calculated, one in respect to x axis (measuring the vertical distance of the two curves) and one in respect to y axis (measuring the horizontal distance of the two curves). The final metric for automatic fusion boundary comparison was the average value of the horizontal MSE and vertical MSE. This metric was proved capable of comparing any two curves of fusion boundaries, regardless of their different shapes and scales; the shapes of the whole profiles of the two curves were compared and the melted area was indirectly compared as well. Fig. 4 illustrates an example of fusion boundary comparison with this metric. The code to implement this metric, as well as the rest of the code of this study, can be found at [16].

The steps to implement this fusion boundary comparison metric were the following:

1. The simulation and experimental fusion boundary profiles should be at the same scale and aligned on the vertical axis. Also, in axisymmetric weld simulations, the simulation fusion boundary should be mirrored at the vertical axis to acquire both left and right profiles.
2. To calculate the horizontal fusion boundary MSE, the right halves of simulation and experimental fusion boundaries were isolated, and their axes flipped (the x axis of the graphs to be used as y axis and vice versa), so for the profiles to form functions.
3. Cubic interpolation was performed to the exact same points of horizontal axis for both simulation and experimental half profiles.
4. The mean square error between the interpolated points (their mean squared vertical distance) was calculated.
5. The steps 2-4 were repeated for the left halves of simulation and experimental fusion boundaries. Then the right horizontal and left horizontal MSEs were averaged to find the total horizontal MSE.
6. To calculate the vertical fusion boundary MSE, the x and y axes remained as they were (no flipping), but only the bottom profile was kept, so that it formed a function.
7. Then, the steps 3, 4 were implemented.
8. Finally, the horizontal and vertical MSEs were averaged to form the total fusion boundary MSE.

[1] mean square error is the average squared difference between some estimated ($\hat{Y}_i$) and actual (Y_i) values, given by the formula $\text{MSE} = \frac{1}{n}\sum_{i=0}^{n}\left(\hat{Y}_i - Y_i\right)^2$.

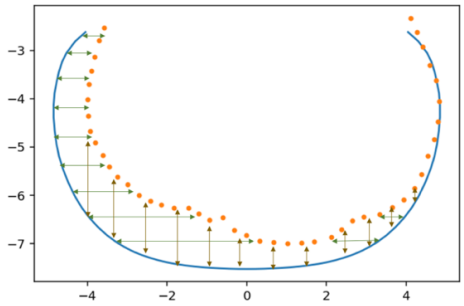

Fig. 4 Visual representation of fusion boundary comparison of simulation solution (effic. = 74%, r_a=1.0, r_l=1.5, r_v=2.5) and experimental fusion boundary. The vertical MSE of this comparison is 0.89, the horizontal MSE is 1.34, and thus the total (averaged) MSE is 1.12.

Many different simulation fusion boundaries were generated from the exhaustive search of heat source radii solutions, and some trends were observed. By increasing only one radius each time and keeping the rest at small values, it was noticed that the increase of vertical radius r_v increased the depth of simulation fusion boundary, the increase of lateral radius r_l increased its width, and the increase of axial radius r_a reduced the melted area a little.

The fusion boundary comparison metric was found to be influenced by all three heat source distribution radii, as it can be seen in Fig. 5. The solution that minimised this metric was (r_a=2.9, r_l=2.2, r_v=1.5).

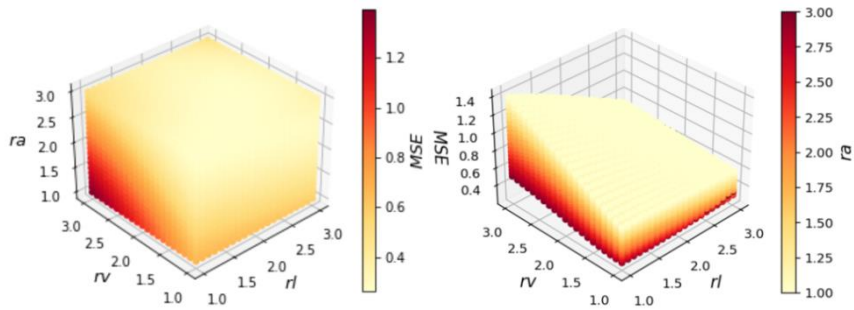

(a) (b)

Fig. 5 Fusion boundary MSE of the exhaustive search of radii interval 1.0-3.0 and efficiency fixed to 74%. In subfigure (a) the MSE is represented by the colour map in a three-axes space of radii values, while in subfigure (b) the MSE is represented by the vertical axis. The minimum MSE value is at (r_a=2.9, r_l=2.2, r_v=1.5).

The thermocouple RMSEs, far-field and near-field, were also examined. For far-field thermocouples the RMSE described by Eq. 2 was used, and the RMSEs of the two specimens 2-1A and 3-1B were averaged. For near-field thermocouples however, a weighted RMSE was used, described by the Eq. 3. Weighted means that, each thermocouple term in the RMSE expression was divided by the total number of

thermocouples that were located in the same side with this thermocouple term (left side, right side, or middle). The reason for this was that the number of near-field thermocouples on the left side of the weld was different to the number of near-field thermocouples on the right side. Since the experimental fusion boundary has not always symmetry about the vertical axis, the thermocouples on the left side of the weld might have different opinion on the heat source parameters than the thermocouples on the right. If a non-weighted RMSE was used, then the opinion of the side with more thermocouples would dominate, and we would not want such bias.

$$RMSE_{weighted} = \sqrt{\{\{[(\Delta T_{TC2,sim} - \Delta T_{TC2,exp}) / \Delta T_{TC2,exp}]^2 + [[(\Delta T_{TC10,sim} - \Delta T_{TC10,exp})/\Delta T_{TC10,exp}]^2 + [(\Delta T_{TC11,sim} - \Delta T_{TC11,exp}) / \Delta T_{TC11,exp}]^2]/2 + [(\Delta T_{TC9,sim} - \Delta T_{TC9,exp})/\Delta T_{TC9,exp}]^2\}/3\}} \quad (3)$$

The weighted RMSE of each specimen 2-1A and 3-1B was calculated and then they were averaged across the two specimens. In the following text, when referring to RMSE of far-field or near-field thermocouples we will mean that Eq. 2 and Eq. 3 were used respectively, and also that the calculated RMSEs were averaged across the two specimens.

The far-field thermocouples showed very low variation of RMSE value with different combinations of heat source radii, as it can be seen in Fig. 6, and they appeared to be mainly influenced by lateral radius (r_l). The near-field thermocouples also showed to have small influence by the heat source radii, as can be seen in Fig. 7, and were found to be influenced more by the vertical and lateral radii (r_l and r_v) rather than the axial (r_a). It should be pointed out however, that these observations were true for the specific interval of solution space that was examined (1.0 - 3.0), and cannot be safely generalised for other intervals or welding cases.

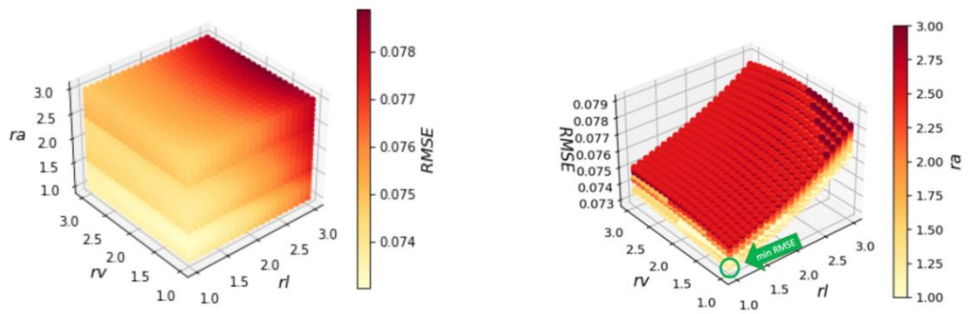

(a) (b)

Fig. 6 RMSE of far-field thermocouples (averaged across specimens 2-1A and 3-1B) of the exhaustive search of radii interval 1.0-3.0 and efficiency fixed to 74%. In subfigure (a), the RMSE is represented by the colour map in a three-axes space of radii values. In subfigure (b), the RMSE is represented by the vertical axis and its minimum value (r_a=1.3, r_l=1.0, r_v=1.0) is pointed out by the arrow.

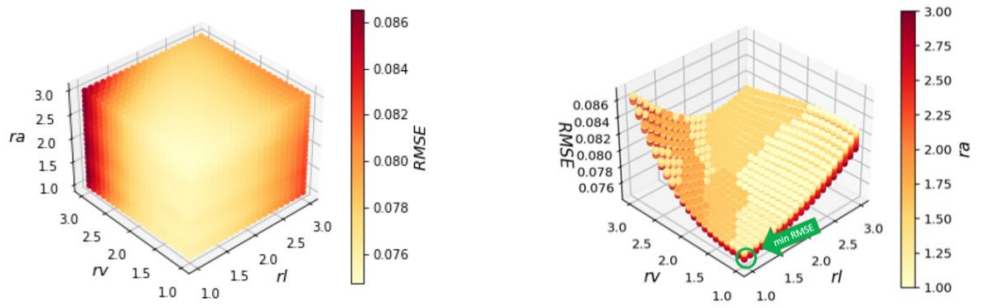

(a) (b)

Fig. 7 Weighted RMSE of near-field thermocouples (averaged across specimens 2-1A and 3-1B) of the exhaustive search of radii interval 1.0-3.0 and efficiency fixed to 74%. In subfigure (a), the RMSE is represented by the colour map in a three-axes space of radii values. In subfigure (b), the RMSE is represented by the vertical axis and its minimum value (r_a=3.0, r_l=1.0, r_v=1.0) is pointed out by the arrow.

It is of interest that both far-field and near-field show preference towards the (r_a=1.0, r_l=1.0, r_v=1.0) corner of solution space. Specifically, the optimal solution according to the RMSE of far-field thermocouples was (r_a=1.3, r_l=1.0, r_v=1.0) and according to the weighted RMSE of near-field thermocouples it was (r_a=3.0, r_l=1.0, r_v=1.0). At this point, let's remind to the reader that, this exhaustive search of heat source radii was conducted with 74% efficiency which was found by arbitrarily fixing the heat source radii to the (r_a=1.0, r_l=1.0, r_v=1.0) vector. So, shall we trust the thermocouples' opinion or shall we first investigate if they are influenced by the arbitrary choice of heat source radii that was used for determining the efficiency? To answer this question, the same procedure was followed, but now by fixing the efficiency with heat source radii vector (r_a=3.0, r_l=3.0, r_v=3.0).

The results showed that we were right to think that the thermocouples' opinions were biased by the choice of radii initialisation vector. After fixing the heat source radii to (r_a=3.0, r_l=3.0, r_v=3.0), the optimal efficiency was found with the same method as before, that is, by minimising the RMSE, but now the optimal efficiency was found to be 72% (instead of 74% that was found previously with fixing the radii to (r_a=1.0, r_l=1.0, r_v=1.0)). Then, the exhaustive search of heat source radii solutions was again performed in the 1.0-3.0 interval for each radius, but with 0.5 step now (less data points than before) to reduce the computational cost. It was found that both far-field thermocouples showed a preference towards the new choice of radii (r_a=3.0, r_l=3.0, r_v=3.0). Specifically, the best solution for far-field thermocouples was (r_a=3.0, r_l=1.0, r_v=3.0) and for near-field thermocouples (r_a=3.0, r_l=1.5, r_v=1.5). On the other hand, the fusion boundary metric again appeared not to be influenced by the arbitral choice of radii, and gave best solution of (r_a=3.0, r_l=1.5, r_v=1.5), which is closed to the previous solution of (r_a=2.9, r_l=2.2, r_v=1.5).

After these observations, it was judged that the best metric for radii determination out of the three metrics, namely RMSE of far-field thermocouples, weighted RMSE of near-field thermocouples, and fusion boundary comparison, was the fusion boundary one. This is because it was the least biased by the initial heat source radii selection of heat

efficiency determination. The thermocouple metrics or any other metric that is a combination of fusion boundary and thermocouple metrics, might shift the radii solution to areas biased by the initial choice of radii to fix the efficiency.

HEAT SOURCE CALIBRATION

The aim of heat source calibration is to find the optimal values of heat efficiency, heat source radii, and sometimes other parameters as well, such as the vertical position of the heat source. By optimal values we mean that, we want the values that would result in a finite element thermal solution as close to the experimental one as possible.

In this research, the heat efficiency and heat source radii (r_a, r_l, r_v) were calibrated for NeT-TG4 specimen. Initially, the heat source radii values were fixed to an arbitrary number (r_a=1.0, r_l=1.0, r_v=1.0) and the optimal efficiency was found (74%). Then, with efficiency fixed, the optimal heat source parameters were determined based on the fusion boundary comparison metric that was developed in this study. The optimal heat source radii found at this stage were (r_a=2.9, r_l=2.2, r_v=1.5). The far-field and near-field thermocouple metrics were not used for heat source radii determination, as they were found to be significantly influenced by the initial heat source radii vector chosen to determine the efficiency. However, it was found that, the fusion boundary metric was slightly influenced by the initial choice of heat source radii as well, since the heat efficiency was slightly different depending on this choice. It was then clear that an iterative process is necessary in order to find the optimal combination of efficiency and heat source radii, until the efficiency value does not change any more. This procedure was followed for the NeT-TG4 specimen and is schematically illustrated in Fig. 8.

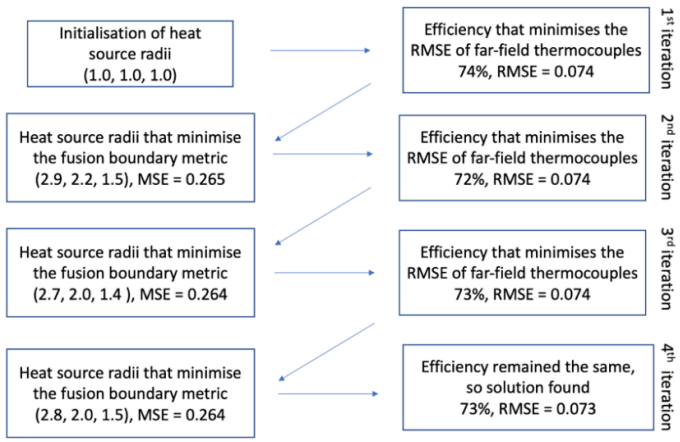

Fig. 8 Heat source calibration iterative process for exploration interval of 2nd iteration 1.0-3.0 for each heat source radius

The interval of exploration for efficiency was 10-100% in all iterations (although very low values wouldn't be realistic). For the 2nd iteration (the numbering of iterations is

described in Fig. 8), the interval of exploration for heat source radii was 1.0-3.0 for each radius. In consequent iterations however, the interval of exploration for heat source radii was reduced, to avoid unnecessary computational cost, and it was selected to include the interval of 10 best solutions (according to fusion boundary metric) of the previous iteration. Also, areas outside this exploration interval were explored, in cases where the solution was close to the boundaries of interval of the previous iteration. Following that method, the exploration interval for heat source radii was (r_a=2.7-3.3, r_l=1.8-2.6, r_v=1.3-1.7) for the 3rd iteration and (r_a=2.5-2.8, r_l=1.8-2.0, r_v=1.3-1.6) for the 4th, with step 0.1. At some iterations the interval of exploration might have been tighter than ideally, but this was to reduce the computational cost of the exhaustive search. The fusion boundary shapes for each solution of each iteration were very similar, and they matched the experimental fusion boundary very well.

The final solution, which was heat efficiency 73% and heat source radii r_a=2.8, r_l=2.0, r_v=1.5, is illustrated in Fig. 9, along with the experimental fusion boundary. The vertical MSE of the two curves was 0.16, the horizontal MSE was 0.37, and their average (total MSE) was 0.26. This MSE value should be considered very low, due to the asymmetry of the experimental fusion boundary about the vertical axis, and also due to the fluctuations of its profile, whilst the simulation fusion boundary profile was symmetrical and smoother.

As for the thermocouple metrics for the final solution (effic.=73%, r_a=2.8, r_l=2.0, r_v=1.5), the RMSE of far-field thermocouples was found to be 0.073 and the near-field thermocouple weighted RMSE was 0.075. Fig. 10 shows that the simulation temperature increases (maximum - initial temperature) versus the experimental temperature increases of thermocouples of the two specimens. As it can be seen, the near-field thermocouples for specimen 3-1B were a bit underpredicted, whilst for specimen 2-1A were a bit overpredicted.

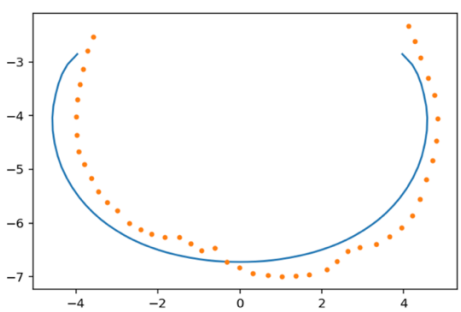

Fig. 9 Final solution of iterative process of radii exploration interval of 2nd iteration 1.0-3.0, that is, efficiency 73% and heat source radii (r_a=2.8, r_l=2.0, r_v=1.5)

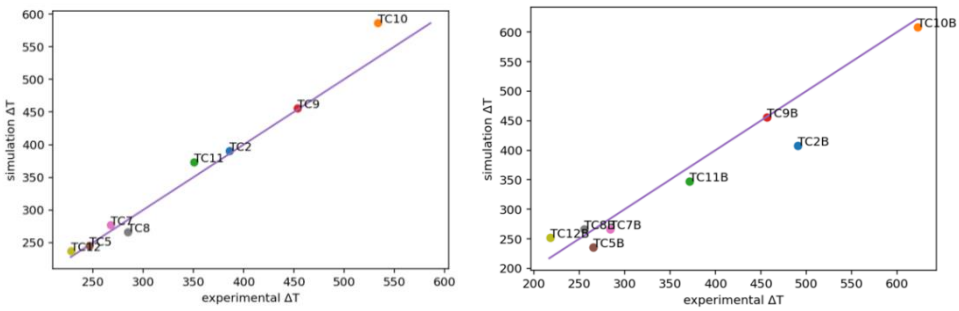

Fig. 10 Thermocouples' experimental versus simulation temperature increases of final solution (effic.=73%, r_a=2.8, r_l=2.0, r_v=1.5) for specimens 2-1A (left) and 3-1B (right)

MULTIPLE GOOD SOLUTIONS

The examination of solution space of the iterative process of fixing the efficiency first and then the heat source radii based on the fusion boundary comparison led to a single area of solution space of best solution. This means that, the problem appeared to have one optimal solution and not many different optimal solutions. Furthermore, the solution space seemed smooth, meaning that, the thermocouple and fusion boundary metrics changed almost continuously with the solution space. However, let's remind the reader that, the interval of radii exploration that we started with (1.0-3.0) was rather small and based on previous experience from the NeT-TG4 project. What would happen if we started with another solution space interval? Could we have many different solutions that appear optimal? To answer these questions, the exhaustive search of solution space was repeated, but now with radii exploration interval 0.1-2.0, with step 0.1. The initialisation of heat source radii vector was again (r_a=1.0, r_l=1.0, r_v=1.0) and hence the initial efficiency was fixed to 74%.

The results showed that the fusion boundary comparison metric gave now a completely different optimal solution of 2nd iteration (r_a=2.0, r_l=0.8, r_v=0.1) compared to the solution of 2nd iteration of previous exploration (r_a=2.9, r_l=2.2, r_v=1.5). The heat efficiency of 2nd iteration was now found 74% (same as 1st iteration), and so the algorithm stopped, giving final solution (r_a=2.0, r_l=0.8, r_v=0.1), as described in Fig. 11. Because the axial radius of the solution was in the upper boundary of exploration interval (r_a = 2.0), if we wanted to be more detailed, the algorithm should had restarted with an expanded exploration interval towards the upper boundary region of r_a, to ensure that the optimal solution would be found for this region of good solutions. Nevertheless, the solution (effic.=74%, r_a=2.0, r_l=0.8, r_v=0.1) had a decent total MSE of 0.35 (average of horizontal and vertical MSEs), but a bit larger than the total MSE of 0.26 of final solution (effic.=73%, r_a=2.8, r_l=2.0, r_v=1.5) of the previous exploration, and its fusion boundary is illustrated in Fig. 12.

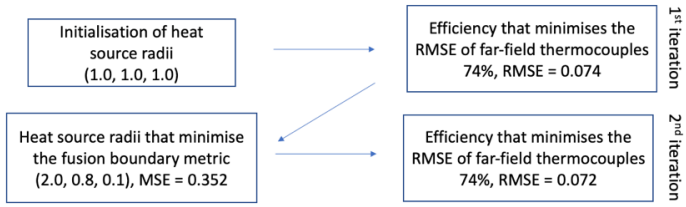

Fig. 11 Heat source calibration iterative process for exploration interval of 2nd iteration 0.1-2.0 for each heat source radius

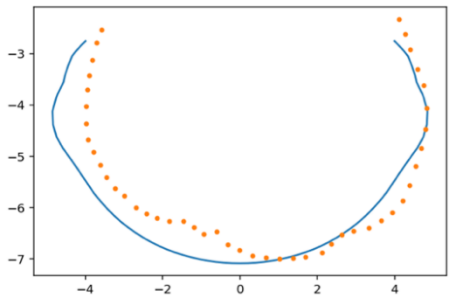

Fig. 12 Final solution of iterative process of radii exploration interval of 2nd iteration 0.1-2.0, that is, efficiency 74% and heat source radii (r_a=2.0, r_l=0.8, r_v=0.1)

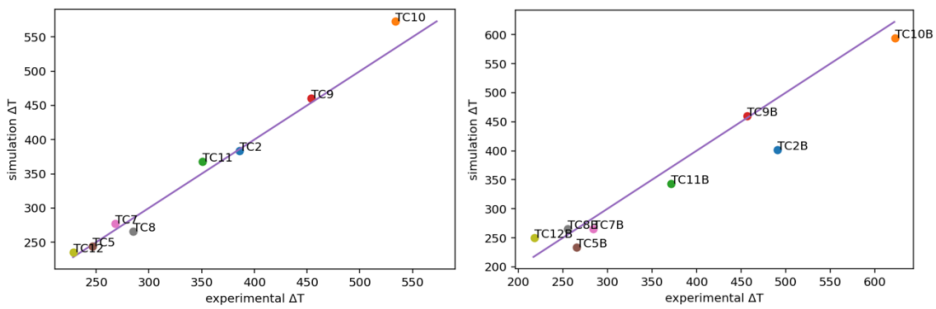

Fig. 13 Thermocouples' experimental versus simulation temperature increases of final solution (effic.=74%, r_a=2.0, r_l=0.8, r_v=0.1) for specimens 2-1A (left) and 3-1B (right)

Regarding the thermocouple metrics, they were found to be very similar across both solutions. For solution (effic.=74%, r_a=2.0, r_l=0.8, r_v=0.1) the far-field thermocouple RMSE was 0.072 and the weighted RMSE value of near-field thermocouples was 0.075, which were almost the same with the previous solution (effic.=73%, r_a=2.8, r_l=2.0, r_v=1.5). Fig. 13 illustrates the simulation temperature increases of this solution and shows that they were very similar with the temperature increases of the previous solution.

According to these observations, in an adequately large interval of exploration, multiple different regions of good solutions might appear. The fusion boundary metric for

the multiple good solutions might be similar. The thermocouple metrics across these solutions might be similar too. In this study, two different good solution regions were identified for NeT-TG4, which were (effic.=73%, r_a=2.8, r_l=2.0, r_v=1.5) and (effic.=74%, r_a=2.0, r_l=0.8, r_v=0.1) (and probably other good solution regions exist for this specimen as well, outside the intervals examined in this study). However, the fusion boundary metric was better for the former solution rather than the latter, and thus it would be justified to choose the (effic.=73%, r_a=2.8, r_l=2.0, r_v=1.5) as the best option.

CONCLUSIONS

The conclusions of this research were the following:

1. The automatic fusion boundary metric that was developed in this study was able to compare all fusion boundary shapes and sizes and was easy to implement, by averaging the MSE of differences of the experimental and simulation fusion boundary curves both in horizontal and in vertical axis. This metric could be used as target value for fusion boundary comparisons in structural integrity assessment guidelines. When deciding the target value for this metric, the experimental fusion boundary asymmetry by the vertical axis should be taken into consideration and also the fluctuations of its profile, as with their increase the value of the metric would increase too.
2. The determination of efficiency before the heat source radii accelerated the heat source calibration process, by reducing the exploration space. The proposed guidelines for automated heat source calibration of heat efficiency and heat source radii can be summarised as follows:
    a. Firstly, an arbitrary vector for the heat source radii is selected, preferably realistic in size, that is, some mm smaller than the width of the macrograph.
    b. Then, the heat efficiency is determined by minimising the RMSE value of far-field thermocouples, as these thermocouples can approximately estimate the heat efficiency regardless the choice of initialising heat source radii vector.
    c. An interval of exploration of possible heat source radii solutions is then selected. The efficiency is kept fixed to the value that was previously determined, and the heat source radii vector that minimises the fusion boundary metric is selected. The thermocouple metrics (far-field and near-field) are not used at this stage to find the heat source radii, since their preferences could be biased towards the initialising heat source radii vector.
    d. The heat efficiency is then recalculated, and an iterative process begins between heat source radii and efficiency calculation, until the efficiency does not change any more. In every iteration, for computational efficiency, the interval of exploration can be narrowed down to regions around the interval of radii value of ‘n’ best solutions of the previous iteration.
3. Depending on the interval of exploration, very different heat source radii solutions, that give almost equally good results, can be found. In contrast to the heat source radii solutions, by following the method of firstly fixing the

efficiency with far-field thermocouples, the solutions for efficiency can deviate only a little.

4. Appropriate optimisation algorithms could be selected to accelerate the automated heat source calibration workflow. The heat efficiency was found to have only one value which minimises the RMSE of far-field thermocouples. Therefore, the exhaustive search could be easily substituted with any optimisation algorithm that searches for one minimum and does not require the function's derivative (e.g., golden-section search). The optimisation of heat source radii is a more complex problem. The fusion boundary metric appears to have a continuous value in the solution space. However, multiple different good solutions seem to exist (many local minima). Therefore, a gradient based optimisation algorithm that does not require the function's derivatives and also that can handle many local minima could be used.

FUTURE WORK

In this study automated heat source calibration was performed with exhaustive search. However, this requires computational time (for this research the computational time was about 5 days). Instead of exhaustive search, optimisation algorithms could be used to find the minima to further accelerate the heat source calibration (particularly useful if large solution space intervals need to be explored) and to ensure that the optimal solution is found. So, future work will be focused on implementation of appropriate optimisation algorithms. Also, future work will include the application of the optimised heat source calibration workflow to new specimens and welding processes so to assess its general applicability.

ACKNOWLEDGMENTS

The authors are grateful and wish to acknowledge the NeT European Network for the provision of data and the protocols. The authors would also like to acknowledge the computational shared facility of the University of Manchester, in which the simulations for this study were run. M. C. Smith, A.N. Vasileiou and D.K. Rissaki are supported by the SINDRI - Synergistic utilisation of Informatics and Data centric Integrity engineering, EPSRC Prosperity Partnership (Grant number: EP/V038079/1) and University of Manchester's Dalton Nuclear Institute.

References

[1] AKRIVOS V., MURANSKY O., DEPRADEUX L., SMITH M.C., VASILEIOU A., DEACONU V., ET AL: 'On the Accurate Prediction of Residual Stress in a Three-Pass Slot Nickel-Base Repair Weld by Numerical Simulations', *Journal of Manufacturing and Materials Processing*, 2022, 6(3):61.

[2] VASILEIOU A.N., SMITH M.C., BALAKRISHNAN J., FRANCIS J.A., HAMELIN C.J.: 'The impact of transformation plasticity on the electron beam welding of thick-section ferritic steel components', *Nuclear engineering and design*, 2017, 323:309-16.

[3] BELOUAH S., BOREL D., DELMAS J., HENDILI S., ROBIN V.: 'Open-source Numerical Simulation Softwares and Skill-Modules for Welding Simulation'.
[4] BELITZKI A., MARDER C., HUISSEL A., ZAEH M.F.: 'Automated heat source calibration for the numerical simulation of laser beam welded components', *Production Engineering*, 2016, 10(2):129-36.
[5] FARIAS R., TEIXEIRA P., VILARINHO L.: 'An efficient computational approach for heat source optimization in numerical simulations of arc welding processes', *Journal of Constructional Steel Research*, 2021, 176:106382.
[6] SHIRAIWA T., ENOKI M., GOTO S., HIRAIDE T.: 'Data Assimilation in the Welding Process for Analysis of Weld Toe Geometry and Heat Source Model', *ISIJ International*, 2020, ISIJINT-2019-720.
[7] PYO C., KIM J., KIM J.: 'Estimation of heat source model's parameters for GMAW with non-linear global optimization - part I: Application of multi-Island genetic algorithm', *Metals*, 2020, 10(7):885.
[8] GU Y., LI Y., YONG Y., XU F., SU L.: 'Determination of parameters of double-ellipsoidal heat source model based on optimization method', *Welding in the World*, 2019, 63(2):365-76.
[9] SMITH M., SMITH A., WIMPORY R., OHMS C.: 'A review of the NeT Task Group 1 residual stress measurement and analysis round robin on a single weld bead-on-plate specimen', *International Journal of Pressure Vessels and Piping*, 2014, 120:93-140.
[10] SMITH M.C., SMITH A.C.: 'Advances in weld residual stress prediction: A review of the NeT TG4 simulation round robin part 1, thermal analyses', *International Journal of Pressure Vessels and Piping*, 2018, 164:109-29.
[11] SMITH M.C., SMITH A.C., OHMS C., WIMPORY R.C.: 'The NeT Task Group 4 residual stress measurement and analysis round robin on a three-pass slot-welded plate specimen', *International Journal of Pressure Vessels and Piping*, 2018, 164:3-21.
[12] SMITH M., SMITH A.: *NeT Task Group 4: Three-Pass Slot Weld Specimen in Austenitic Stainless Steel*, Issue 1, Appendix F: As-installed thermocouple positions and their impact on measured temperatures, 29/9/2009.
[13] Featplus Limited, Feat-Wmt: *Weld-Modelling Tool User Guide*, 2019.
[14] MURANSKY O., BENDEICH P.J., SMITH M.C., KIRSTEIN O., EDWARDS L., HOLDEN T.M., editors: 'Analysis of Residual Stresses in Three-Pass Slot Weld (NeT-TG4): Finite Element Modelling and Neutron Diffraction', *Pressure Vessels and Piping Conference*, 2010.
[15] MURÁNSKY O., SMITH M.C., BENDEICH P.J., HOLDEN T., LUZIN V., MARTINS R., ET AL: 'Comprehensive numerical analysis of a three-pass bead-in-slot weld and its critical validation using neutron and synchrotron diffraction residual stress measurements', *International Journal of Solids and Structures*, 2012, 49(9):1045-62.
[16] https://github.com/dimitrarissaki/establishing_an_automated_heat_source_calibration_framework.git